Influence of Annealing Treatment on Si Morphology and Strength of Rapid Solidified Al-12 wt.% Si Powders

Leonardo F. Gomes [a], J. E. Spinelli [a,*], A-A. Bogno [b], M. Gallerneault [c] and H. Henein [b]

[a] Department of Materials Engineering, Federal University of São Carlos, São Carlos, SP 13565-905 Brazil.

[b] Department of Chemical and Materials Engineering, University of Alberta, Edmonton, AB T6G 2G6 Canada.

[c] Alcereco Inc, Kingston, ON, Canada

Abstract

An experimental study is reported on heat treating rapid solidified Al-12 wt.% Si alloy with 355-425 μm powder size. Fast heat treatments at 813K revealed morphological shifts of eutectic Si from the as-atomized condition to those after annealing. The Si network of the as-atomized samples showed a fine dispersed coral fibrous architecture. This feature via rapid cooling brings the prospect of quickly disintegrating and spheroidizing Si in a few minutes without chemical modification. By adopting different exposure times, it was possible to investigate fragmentation and coarsening of the eutectic Si. The integrity of the Si network is very sensitive to the Si spheroidization treatment transforming into a network of round Si particles. It is also seen that the material softens in the earlier stages of heat treatment, especially after 2 minutes of heat treatment. The breakdown in Si rods in a rapidly solidified alloy is shown to take place with a mixed mechanism of interface or internal rod diffusion and diffusion of supersaturated Si through the α primary phase to the Si rods in the eutectic. The quantitative analysis of the microstructures coupled with an analytical strengthening model resulted in good agreement between experimental and calculated data.

Keywords: Al-Si; Impulse Atomization; Annealing; Strengthening model; Microstructure; Hardness.

* Corresponding author → E-mail address: spinelli@ufscar.br (J.E. Spinelli)

1. Introduction

Control of the microstructure size and morphology of Si in Al-Si alloys is essential in order to meet the progressively increasing demands for automotive and aerospace applications [1,2]. The binary Al-Si system is a eutectic system whose eutectic point is about 12 wt% Si at 850K [3,4]. Two strengthening mechanisms are mainly reported for this material [5,6]. The first is by the addition of other elements such as Mg and Cu, followed by heat treatment. The second by using rapid solidification techniques such as melt spinning, atomization, laser surface remelting, among others. Both approaches lead to a refinement of the microstructure. Addition of eutectic modifiers (i.e., Na, Sr, B, Ti) can either decrease the size of the eutectic grains at moderate cooling rates or alter the eutectic Si morphology [7,8]. The addition of these elements requires much control in order for them to be effective. This is due to possibility of vaporization and oxidation of these added elements, which could result in their loss during operation [9,10].

An increase in cooling rate may refine the alloy microstructure. As a consequence, rapid solidified Al-Si parts can exhibit improved mechanical properties. Processes such as Selective Laser Melting (SLM) are characterized by very high cooling rates (10^3-10^8 $K.s^{-1}$) due to the concentration of laser heating in a very small volume of material together with short laser-material interaction time [10]. Al-Si alloys are considered classic SLM materials [11]. The occurrence of subsequent thermal cycles may lead to phase evolution, as for example, spheroidization of Si phases. This is an intrinsic characteristic of this technique, in which thermal history is typified by alternating fast heating and cooling rates. [11].

Traditional solution heat treatment and spheroidization treatment have already been evaluated for various rapid solidified Al-Si based alloy components. Zhou *et al.* [12] observed that the Si content in α(Al) exceeded the Si solubility expected in the equilibrium conditions. For the tested Al-10SiMg SLM alloys, coarsening and spheroidization of the eutectic structure were observed after conventional treatment. Liu et al. [13] stated that the high hardness of 130 HV may be achieved in Al-7%Si alloy if an optimized microstructure is formed. In this case, the Al-Si alloys having nanoscale Si precipitates were prepared through high pressure solution treatment (HPST) followed by low aging treatment. The HPST method consisted of heating the samples to 700 °C under an isostatic pressing pressure of 6GPa.

This condition is held for 1 h followed by water quenching to room temperature. This work compared the contributions of solid solution hardening and precipitation hardening to the strength of the Al-7%Si alloy. It was stated that the precipitation hardening appears to be the major strengthening contribution after aging for 1800 s.

Prashanth et al. [6] fabricated Al-12wt%Si specimens by SLM. After characterizing an extremely fine cellular microstructure which was decorated with elongated Si platelets in the cell boundaries, it was demonstrated that annealing treatments could be pre-programmed in order to attain a proper balance of strength and ductility in the Al-12wt%Si SLM samples. An increase in annealing temperature (from 473K to 723K for 6 hours) resulted in a coarser microstructure. Si was observed to be rejected from the supersaturated Al to constitute small Si precipitates.

Li et al. [10] produced ultrafine eutectic Al-12wt%Si alloy, which revealed excellent mechanical properties by using SLM coupled with solution heat treatment. The as-fabricated microstructure was composed of nano-sized Si enveloping a supersaturated α(Al) matrix. According to this work, the refined spherical morphology of Si gave reason for the excellent tensile properties. During solution treatment at 773K for up to 4 hours Si precipitation and Si coalescence have been observed simultaneously with decreasing Si content in the matrix. STEM-EDX maps of the Al and Si elements in this Al-12wt%Si SLM alloy showed a decrease in the concentration of Si in Al from 7.2wt% to 2.2wt% after the solution treatment at 773K for 15 min.

Heat treatment of the alloy at 450-520°C for several hours is time-consuming and costly. In this regard, novel approaches are required coupling adequate as-fabricated microstructure, i.e., control of the eutectic Si morphology, size and distribution, with Si spheroidizing through short treatment times. There are very few studies addressing fast silicon spheroidization treatment (SST) of Al-Si based alloys. In addition, works dedicated to the fast SST of rapid solidified eutectic Al-12wt%Si alloy have not been developed so far. Such lack of knowledge regarding rapid solidified Al-Si alloys is quite unexpected considering that such alloys are very common materials in several component applications in both automotive and aerospace industries. Furthermore, the mechanism associated with Si spheroidization has not been delineated in the literature.

Existing research efforts reported in the literature are dedicated to fast SST in Al-Si alloys but emphasize spheroidized Si and their growth in commercial compositions. One of these few works by Haghdadi et al. [14] has shown that the high strains induced during accumulative back extrusion (ABE) of A356 aluminum alloy accelerated the kinetics of silicon spheroidization at 813K. The amount of 200ppm of titanium (Ti) was added in the alloy composition to promote refinement of the microstructure. The heat treatment improved the elongation at the expense of the tensile strength. The best compromise of tensile properties for the A356 alloy was achieved by coupling ABE+2min spheroidizing at 813K. Before ABE processing, the Si fibers generated by thixo-casting exhibited a mean diameter of about 0.5 μm in cross section and a length in the range of about 1-5 μm.

Ogris et al. [15] coupled strontium (Sr) modification of the A356 aluminum alloy with silicon spheroidization through high temperature heat treatment. The direct result of the heat treatment was the modification of the Si corals morphology into spheroids. The short heat treatment times were due to the coral-like morphology of the modified eutectic silicon. The Si coral fibers were reported as exhibiting a mean diameter of about 0.4 μm. This morphology facilitates the disintegration of silicon and further spheroidization because of a high density of crystal defects characterizing the formed shape. Such defects are terminations, kinks, and striations which are potential points for fragmentation during heat treatment. Highly controlled processes of chemical modification may be put in practice in order to generate the aforementioned features.

In the current study, Al-12wt% Si powders of size 355-425μm were generated by impulse atomization (IA) under helium atmosphere. Firstly, the as-fabricated eutectic Si morphology and size were investigated. Secondly, the analysis of the powders after different exposure times at 813K was performed by measuring the Si size and solute content in α(Al). The integration of optical microscopy (MO), hardness (HV), scanning electron microscopy (SEM) and transmission electron microscopy (TEM) as well as theoretical analysis of Si spheroidization will provide a framework to understand the changes of Si network from coral fibrous to rounded architecture. In addition, the impact of solid solution hardening and Si eutectic hardening on strength for various exposure times will be

considered. Such a study will form the basis for understanding the contributions of alloying elements on Si spheroidization.

2. Experimental procedure

Rapidly solidified Al-12 wt% Si powders were prepared by impulse atomization (IA) under helium atmosphere from 99.99 wt% pure Al and 99.99 wt% pure Si. The principles of IA and the details of the facility are explained elsewhere [16,17]. The solidified powders were washed, dried and separated into various size ranges. For the present work, the range of 355-425 μm was investigated. After IA, portions of the as-atomized powders were subjected to a heat treatment at 813K for various times of 1 min, 2 min, 4 min and 6 min. Subsequently, the heat treated specimens were immediately quenched in room temperature water.

Microstructures and morphologies of the as-atomized and heat treated specimens were observed using a BX61 Olympus optical microscope. The powders were conventionally prepared for metallography and etched with Keller's reagent for 10-20s. SEM analysis with both Secondary Electrons (SE) and In-Lens detector modes were carried out on the etched samples (HC*l* during 3 minutes). The instrument used was a Zeiss Sigma Field Emission SEM equipped with a Bruker energy dispersive X-ray spectroscopy (EDS).

The length-scale of the eutectic was determined by either measuring the Si spacing, λ, or the Si diameter, D. These measurements were made using the line intercept method [18,19] in both the as-atomized and heat treated powders.

The Si content in solid solution in α(Al) was investigated using transmission electron microscopy (TEM) and the scanning transmission electron microscope (STEM) mode. The instrument used was a FEI TECNAI G² F20 HRTEM. The samples were mapped using a high-angle annular dark-field (HAADF) imaging in the STEM. Energy-dispersive spectroscopy (EDS) was used to evaluate the Si content in α(Al) of each sample.

In order to prepare the Al-Si powders for TEM analysis, Gatan G-1 epoxy (Gantan Inc., CA, USA) was used. This epoxy was mixed individually with portions of as-atomized powders (0 min) and some 6min heat treated samples. Three discs of 3 mm outer diameter for each condition were prepared. And the discs were ground, dimpled, and ion milled to electron transparency, following the standard procedures for preparing TEM samples from bulk materials [20]. A precision ion polishing system or PIPS (Model 691, Gatan) was used. These Al-12wt%Si alloy samples demonstrated to be stable during ion milling and when exposed to the electron beam in the TEM.

Vickers microhardness (HV) measurements were applied on the cross sections of the Al-12wt%Si alloy specimens along 10 different powders per condition with a load of 50 gf for a dwell time of 15 s. The hardness tester used was a Buhler VH 3100 microhardness machine.

Li et al. [21] stated that the strengths of Al-based alloys (σ) are mainly contributed by the following three mechanisms: precipitate strengthening ($\Delta\sigma_{Si}$), solid solution strengthening ($\Delta\sigma_{SS}$), and the aluminum matrix ($\Delta\sigma_{Al}$). Thus, the overall strength of an aluminum alloy yields:

$$\sigma_y = \Delta\sigma_{Si} + \Delta\sigma_{SS} + \Delta\sigma_{Al} \quad (1)$$

Considering that the Si particles in the present work are of relatively large size, the Orowan bowing mechanism is valid, in which the following equations can be used for calculations:

$$\Delta\sigma_{Si} = \frac{0.84MGb}{2\pi(1-\upsilon)^{1/2}\lambda}\ln\frac{r}{b} \quad and \quad \lambda = r\left(\frac{2\pi}{3f}\right)^{1/2}, \quad (2)$$

where M is Talor factor (3.06 [22]), G is shear modulus of Al matrix (30GPa [23]), b is Burgers vector (0.286nm [22]), *v* is Poison ratio (0.347 [24]), λ is interspacing of Si, r (D/2) is average radius of Si and f is volume fraction of Si. These last three parameters (λ, r and f) were determined from experimental measurements on the microstructures of the Al-12wt%Si alloy.

Si solute in solid solution in α(Al) can also promote solid solution strengthening ($\Delta\sigma_{SS}$), which can also be estimated from:

$$\Delta\sigma_{SS} = HC^{\alpha} \quad (3)$$

where C is the Si content in wt%, which was measured by STEM and SEM in the microstructures regarding each evaluated condition in the present work. H and α are constants [25].

For the strength of Al matrix, $\Delta\sigma_{Al}$=38 MPa considering the value for a commercial pure AA1100-O alloy given in the literature [26].

3. Results and discussion

A. Characterization of microstructure

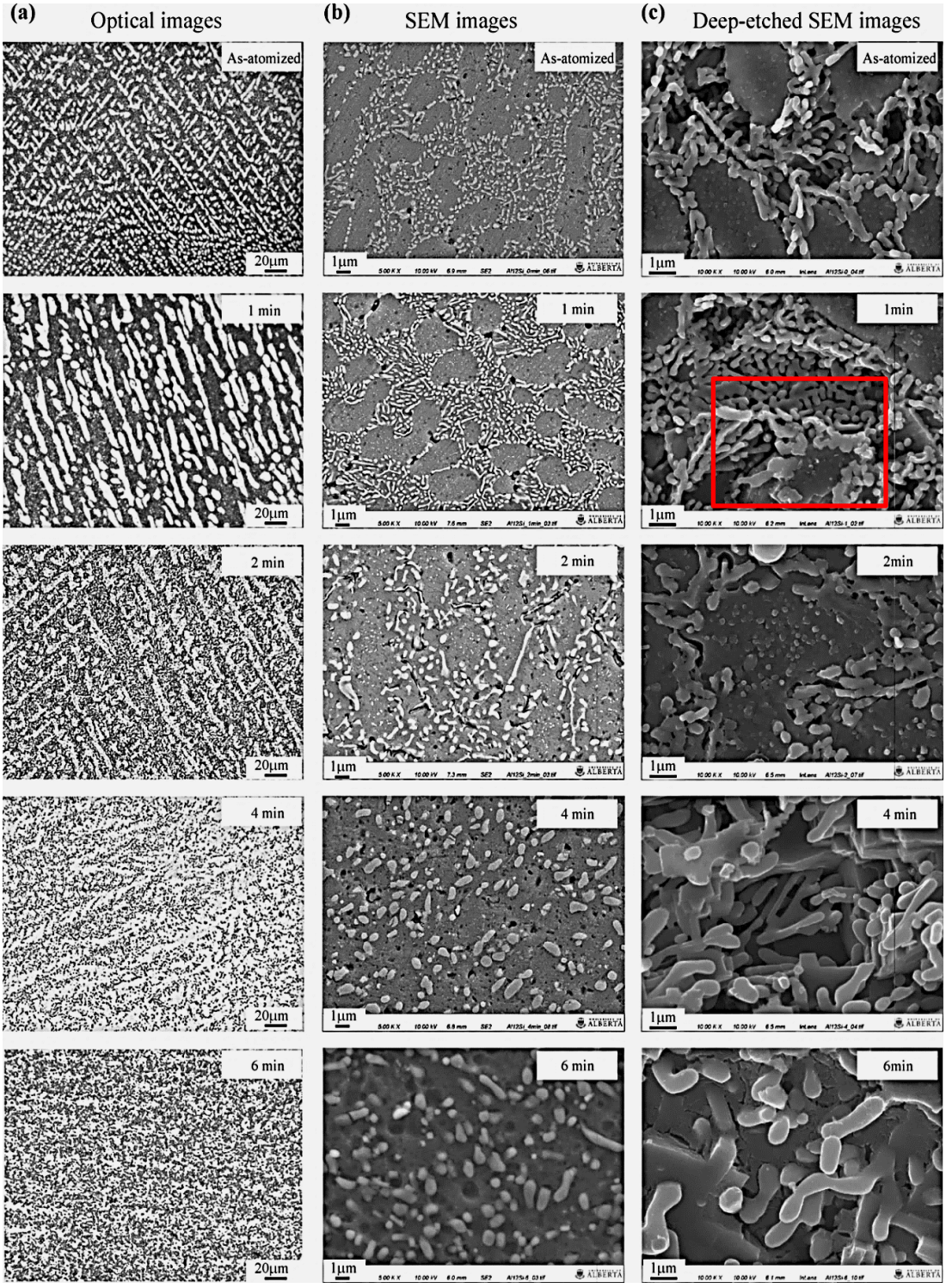

Fig. 1. Representative (a) OM, (b) light-etched SEM and (c) deep-etched SEM micrographs of the as-atomized and heat treated Al-12 wt% Si alloy specimens for different heat treatment times.

Fig. 1 shows the microstructural features of the Al-12 wt%Si alloy as-atomized and heat treated powders using three different magnifications. Each one allows a different aspect of the microstructure to be visualized. Two basic features of the microstructure are observed in Fig. 1: one is composed of the fine α-Al matrix and the other is composed of the eutectic, α–Al+Si, enveloping the α-Al phase.

Each row of images in Fig. 1 refers to a certain processing stage, which means as-atomized condition and heat treated samples at 813K for different exposure times from the top to the bottom in Fig. 1. Such a complete map of microstructures shows not only the morphological and size changes of Si in etched and deep-etched samples by SEM but also the gradual destruction of the dendritic structure until its complete absence for the 6 min treated sample as observed by OM (images at the left in Fig. 1).

The integrity of either the dendritic arrangement or the Si network during heat treatment depends upon the refinement of the microstructure. Fast processes such as IA are able to severely refine the dendrite arms as can be seen in Fig. 1. As such, it makes sense to assume that the smaller the dendrite branches, the faster diffusion process will proceed in the course of destruction of the dendritic array, as can be observed in the samples treated for 4 min and 6 min, which show no more evidences of dendrites.

The change in the Si morphology is of particular interest. This is because such particles can only be partially dissolved in (Al) during long-term homogenization treatments. Furthermore, the shape of Si is able to tailor the alloy mechanical properties [2, 27, 28].

The growth of Si in rods and progressive subdivision under cylinders is considered the ideal shape for fragmentation at the start of heat treatment. In contrast, plate-like particles would not be fragmented as easily during heat treatment because of their smooth planar surfaces [29]. Ogris et al. [15] stated that the branches of the Sr-modified silicon corals could be simply seen as interconnected cylinders. Such morphology can be seen in Fig. 1(c) for the deep etched samples. However, it has been obtained without any chemical modification. This is very positive in the sense that the addition of modifiers as sodium to Al-Si alloys has some drawbacks, such as fading rapidly due to evaporation; difficulty in storing and handling; difficulty in controlling additions can lead to overmodification; and

can increase porosity. The addition of strontium may result in an increase of hydrogen content and can increase porosity and have a long incubation period [30, 31].

The processes of fragmentation, agglomeration and spheroidization of Si particles are directly related to the diffusion of Si atoms. It appears that during heat treatment Si particles break-up into multiple smaller crystals. Each of these may strive to attain a rounder shape during the time available. Higher times of heat treatment appear to increase the degree of roundness of the Si particles.

The evolution of Si network for the various employed times shows different eutectic length-scales as can be seen in the SEM images in Fig. 1(c). The Si particles generated by IA tended to transition from the coral to round shape and coarsened with time.

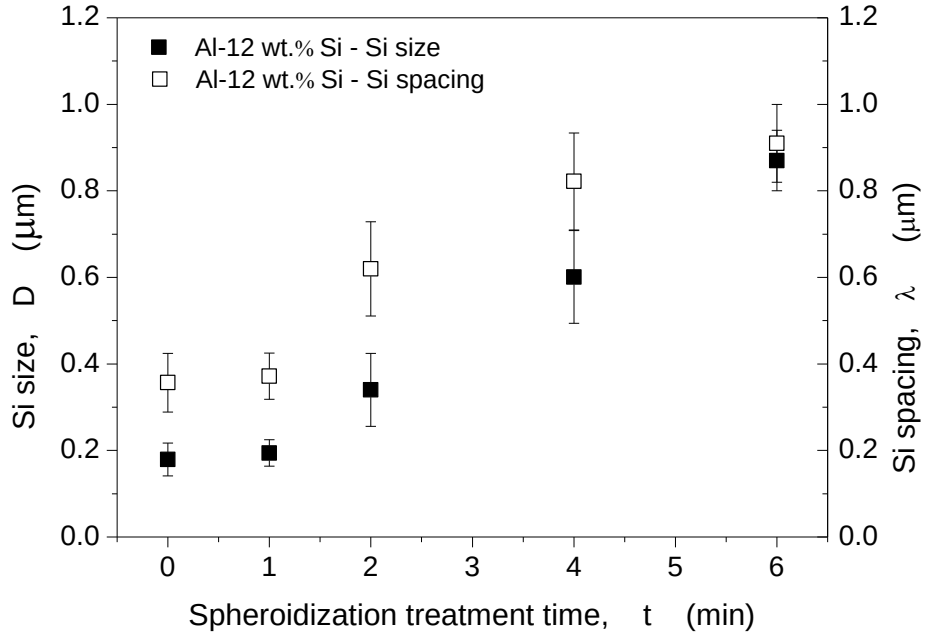

Fig. 2. Variation in range of the Si spacing (λ) and Si size (D) as a function of the annealing treatment at 813K for various times, t, for the Al-12 wt%Si of size 355-425μm generated by impulse atomization under helium atmosphere.

Interparticle Si spacing, λ, was measured for the powder samples generated by heat treatment at 813K for various times as can be seen in Fig. 2. Also, as-atomized samples were examined (referred as 0 min point in the graph). The size, D, of the Si particles after the different heat treatments is also inserted in Fig. 2. Both plots show a variation of the average values along with their standard deviations established for the Al-Si powder of size 355-425μm.

According to Haghdadi et al. [14] the main driving force for coarsening of Si particles is a reduction in surface energy. In this case, a small number of large precipitates contain less interface area if compared to the Si network of small particles. According to Ho and Weatherly [32] spheroidization in Al-Al_2Cu eutectic may be affected by the continued migration of the triple point junctions within the plate at the end of each sub-boundary. Also, these authors [33] demonstrated that the kinetics of spheroidization is accelerated due to the high angle boundaries in the Al_2Cu phase. This mechanism was approached by Conlon et al. [34] after hot pressing rapid solidified Al-Cu powders at 70 MPa and 773 K for 2 hours in a closed graphite die. During long-term annealing at 803 K after hot pressing, a substantial Al_2Cu coarsening was observed. Weatherly [35] stated that parallel rods faceted fibers are stable against perturbations during heat treatment. In this sense many rod eutectics show shape stability (e.g., Al-Al_3Ni) but faults in the microstructure can highly accelerate the coarsening rates.

It can be noted that the Si particles in the as-atomized condition have D and λ values relatively close to those determined for the as-treated samples for 1 min and 2 min, as can be seen in Fig. 2. Based on the mentioned data, it is possible that both fragmentation and coarsening mechanisms balance each other out under such time duration, resulting in similar values for D and λ. The initial fragmentation stage is particularly related to the average interparticle spacing, λ. A fine dispersion of particles, as that observed in the present rapid quenched powders (i.e., λ=0.35 μm), could favor the premature start of the coalescence process. The formation of short cylinders is barely observed in the samples treated for 1 min. (see Fig. 1) whereas they can be clearly seen in the sample after 2 min. This is because in reality the processes of fragmentation and spheroidization happened concurrently for such a particular condition.

Weatherly [35] established a wavelength of $9r_0$ in order to categorize the breakdown of rods through the development of perturbations, where r_0 is the rod or fiber radius in the initial phase of the heat treatment. Fibers having curvature at the interface can be seen in Fig. 1(c). Two groups of eutectics were reported whose perturbations develop rapidly. These are Cu-Cu_2S, Cu-Cu_20 and $Fe_{1-x}S$-Fe; and those whose perturbations progress much more slowly, with a greater variation in the

wavelengths considering the dominant fluctuations, that is, Al_3Ni-Al and NiAl-Cr. The wavelengths around '9 r_0' characterize the first category, which should favor the breakdown of rods and accelerate spheroidization. In contrast, two times higher values of about 17 r_0 are related to the eutectics of the second category. In this case, the breakdown of rods is inhibited as a result of both external volume diffusion and interfacial or internal volume diffusion.

In the present results, 25 measurements of the wavelength were made from SEM images. The wavelength was found to be about 0.577 μm with a standard deviation of 0.156 μm. The wavelength to radius (r_0) ratio of the Si in the initial phase of heat treatment was around '6.4' (i.e., 6.4 r_0 ±1.7). Even though this value is smaller than the expected value of ~9r_o for interface and volume diffusion through the rod (Si in this case), visual observations of the microstructures in Fig.1 indicate that the wavelength of Si decreases with increasing heat treatment time. The present results confirm that fragmentation started during the first 1 min of heat treatment (see Fig. 1(b), the bottom center of the image with highest magnification). In addition, the presence of fibrous terminations having small radii of curvature can also be seen in Fig. 1 (c). This feature is recognized by accelerating coarsening at high temperature [36]. It is therefore likely that this mechanism played a role in the spherodization of the Si, but there is clearly an additional mechanism to consider. This is further discussed below.

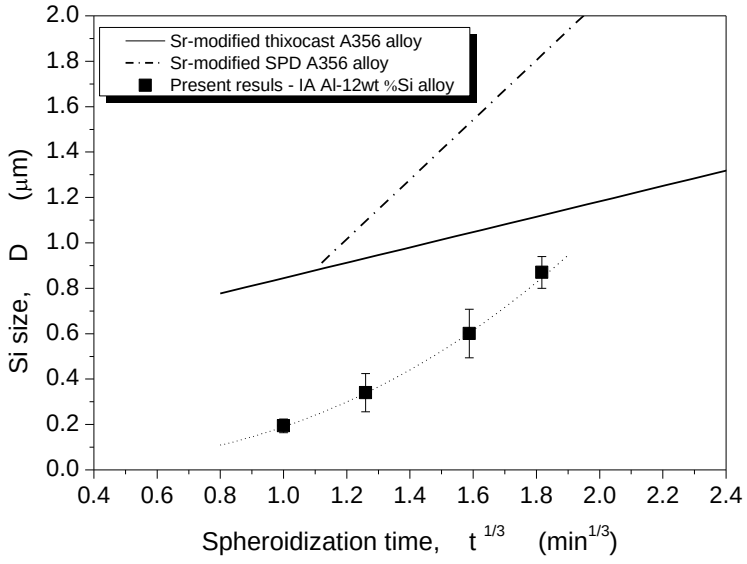

Fig. 3. Plot showing comparison between the Si size with time in the present investigation (i.e., rapid solidified powders) and those found in the literature for the A356 Al alloy generated under different manufacturing routes. Solid and dash-dot lines are from ref. [14].

In the case of the coral fibrous morphology of Si generated by adding modifiers in Al-Si alloys [14,15], sizes of about 400 nm and 500 nm have been reported. In the present investigation, the Si fibers generated by impulse atomization exhibited a mean diameter of about 180 nm in cross section, which is 2.5 times lower than those reported so far.

Fig.3 shows that the value of D increases due to the coalescence of the particles. Significant changes take place after the 2nd minute of heat treatment. Before this point, the intensity of the process is less expressive. The relationship of the Si size *vs.* the cubic root of the time expresses the changes in D with increasing time as defined in Fig. 3. The processes of patterning and changes of Si shape have been facilitated for very short times since the value of diffusion path at 813K is significantly higher than the average interparticle spacing. According to Glazoff et al. [29] when T>773K, the value of the diffusion path exceeds 1 μm.

For comparison purposes, additional growth kinetic relationships of the eutectic Si have been included in Fig. 3. These lines from literature [14] are related to the behavior derived during heat treatment of Sr-modified thixocast and severe plastic deformed, SPD, A356 alloy, which have been also soaked at 813K for short duration times. Both evolutions refer to Si spheroidization treatments in components produced under conditions other than rapid cooling techniques. Although Mg-content of the commercial alloy makes a comparison difficult to be established, this kind of comparison appears to be interesting in terms of the differences in the description of the Si size against time. The relationship derived for the rapid quenched powders examined in the present investigation may not be represented by a linear regression, as stated in the other two cases. This is because proportional relation between D and $t^{1/3}$ may not be established with the present experimental scatter for the Al-12wt %Si alloy as can be seen in Fig. 3. This explains an extra supply of Si atoms diffusing out of the cores of dendrites. As a consequence, larger particles tend to grow and prevail, replacing the smaller ones. It appears that the increase in the kinetics of coarsening is a result of the high solute content within the α-Al matrix achieved during IA. The proper evaluation of the Si content in solid solution as a function of the different treatment durations of the Al-12wt %Si powders will provide more evidence to understand the alloy microstructures and their strengths, as will be seen next.

B. Advanced SEM and TEM analysis

Fig. 4a shows typical SEM micrographs of the investigated Al-12wt %Si samples. Within the micrographs some representative microprobe points, at the center of the α-Al islands, are shown. The points indicate where the EDS analyses were carried out. Fig.4b shows the variation of Si-content in the α(Al) solid solution at different thermal histories (as-atomized powders (treatment time = 0 s) and the heat treated samples at 813K for various durations of 1 min (60s), 2 min(120s), 4 min(240s) and 6 min (360s)) as obtained by the EDS analyses. It is worth noting that a considerable amount of Si is found embedded in the solid solution aluminum matrix especially for much shorter times and non-treated samples. It appears that during Si fragmentation stage for the shorter treatment times of 1 min (60s) and 2 min (120s), there is still a high Si-content within the α(Al) solid solution. On the other hand, for higher durations, corresponding to the Si coarsening stage, the Si-content in the α(Al) solid solution tends towards the equilibrium maximum solubility value of 1.65wt % as predicted by the Al-Si phase diagram at the eutectic temperature.

According to the Fick's second law, higher treatment times at a given temperature allow the diffusion to be reduced with the decrease of the concentration gradient. Assuming that the solute atoms are distributed evenly, an increase in the diffusion time will have negligible effect on the composition segregation, and the segregation extent will not have a further improving.

Fick's second law [37-40] is used to describe the time for the supersaturated Si to diffuse out of the cores of the α(Al) phase , with δ, the microsegregation index, given by equation (4).

$$\delta = \frac{(c_M^t - c_m^t)}{(c_M^0 - c_m^0)} = \exp\left(-\frac{4\pi^2 D_s t}{\lambda^2}\right), \quad (4)$$

where c_M and c_m are the maximum and minimum Si contents. Zero (0) corresponds to the time the heat treatment was begun; t is the diffusion time; D_s is the diffusion coefficient of Si in Al at 813K of 5 x 10^{-13} $m^2.s^{-1}$ and λ is the α(Al) spacing. The minimum Si content, c_m, is the α-eutectic in equilibrium of 1.65 wt% Si.

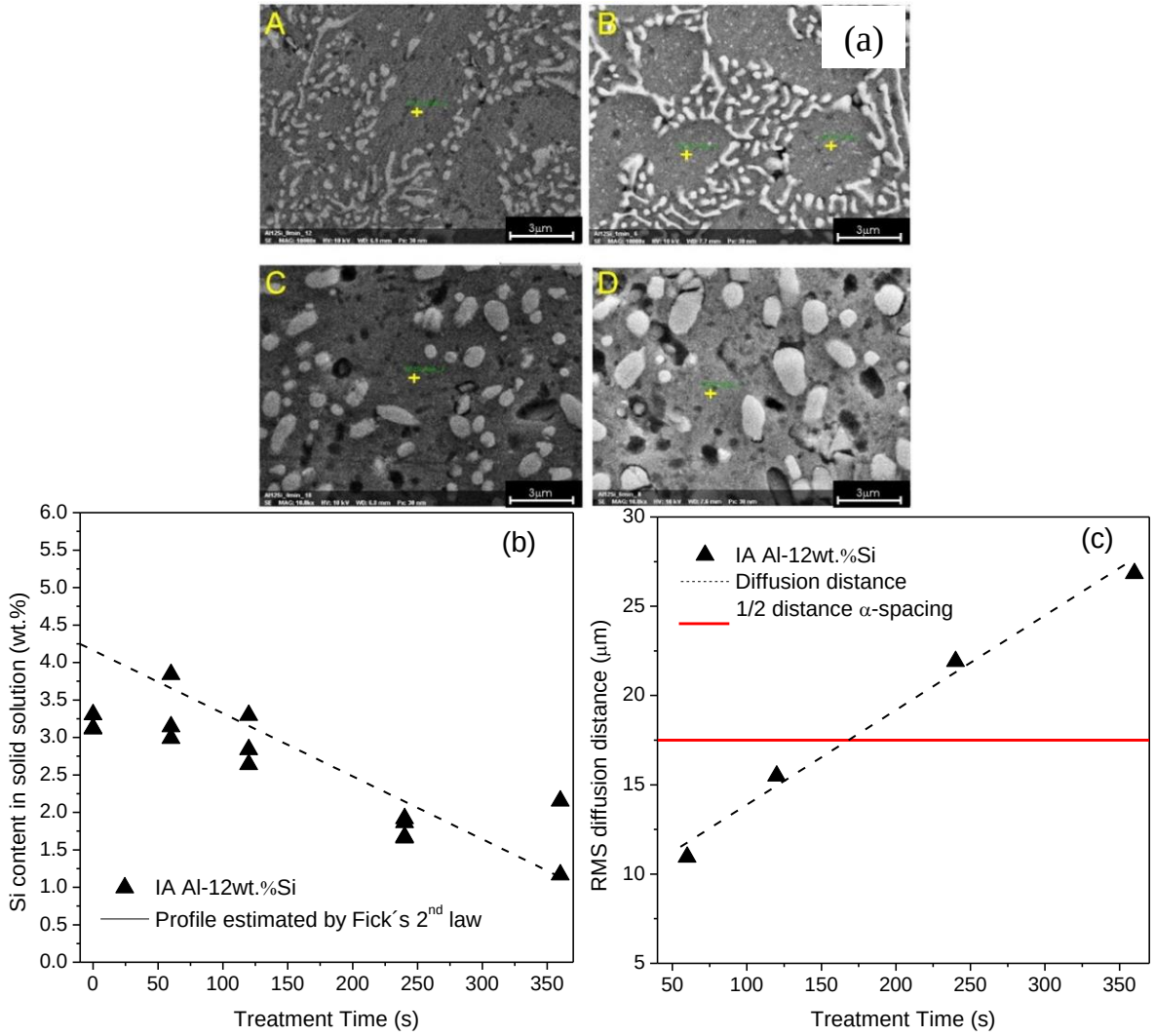

Fig. 4. (a) SEM images through SE mode indicate the evaluated microprobe points emphasizing the composition of the α-Al area within the microstructures. (b) Experimental variation of silicon content in solid solution of the as-tested Al-12 wt% Si alloys samples corresponding to treatment at 813K for various times (i.e., A - 0min; B - 1min; C - 4min and D - 6min). (c) Variation of RMS diffusion distance of Si in α(Al) with treatment time.

The solute profile predicted by the Fick's second law is plotted in Fig.4b (dash line), as can be seen, the experimental variation of Si-content in the α(Al) solid solution with treatment time is in very good agreement with the diffusion model given by Fick's second law after the first minute of heat treatment. Thus, it is likely that in the early stages of heat treatment, the interface or volume diffusion in the Si rod dominate the spheroidization process. At later stages, however, the diffusion of Si from the primary α(Al) contributes to the Si spheroidization. The results shown in Fig. 4b suggest that the

microstructure refinement (i.e. a fine cell spacing of the primary phase) can greatly shorten the diffusion time. As a consequence, the percentage of δ will tend to zero in a duration as short as 6 min. This explains the rapid homogenization observed here. Thus, the breakdown in Si rods in a rapidly solidified alloy will take place with a mixed mechanism of interface or internal rod diffusion and diffusion of supersaturated Si through the α primary phase to the Si rods in the eutectic.

The results shown in Fig.4b are corroborated by the variation of the Root Mean Square (RMS) diffusion distance of Si in the α(Al) solid solution at 813K for different treatment times. Indeed, Fig.4c. shows that the variation of RMS diffusion distance of Si in α(Al), $\sqrt{4D_s t}$, with treatment time compares very well with the Si evolution in α(Al). In the early stages of heat treatment, the RMS diffusion distance of Si in α(Al) is smaller than the half-distance of α(Al)-spacing (center-to-boundary between two α(Al) phases). And, at later stages, the RMS diffusion distance of Si is shown to be larger than the half-distance of α(Al)-spacing, suggesting that for the given treatment times, Si can very well diffuse out of the α(Al) solid solution and contribute to the spheroidization at the boundaries.

A more reliable analysis of the microstructure was carried out through transmission electron microscopy (TEM). Fig. 5 shows regions of the microstructures of the Al-12wt%Si alloy through STEM high-angle annular dark-field (HAADF) and the X-ray (EDS) elemental points for Al and Si. The Si particles can be seen in detail at higher magnifications for the samples after IA (i.e., 0 min) and after 6 min of heat treatment at 813K. It can be seen that the smaller eutectic Si particles were developed in the as-atomized sample.

The STEM-EDS analyses (inset tables in Fig. 5) indicate the presence of 4.49wt% and 1.29/1.62wt% Si in α-Al spots for the samples after IA and after 6min respectively. IA sample showed a considerable amount of Si embedded within the α-Al matrix. These results confirm the experimental points in Fig. 3. Liu et al. [13] solution treated the Al-7wt% Si alloy under high pressure and traced a solubility evolution of Si for heat treated samples at 443K for various periods of time. High Si solubility of about 7wt% Si was observed for the as-processed sample decreasing for values between 1wt% and 2wt% Si for higher aging times.

The quantification of Si solubility was performed in the as-fabricated powders and in those subjected to heat treatment at 813K for modeling purposes as will be described in the next section.

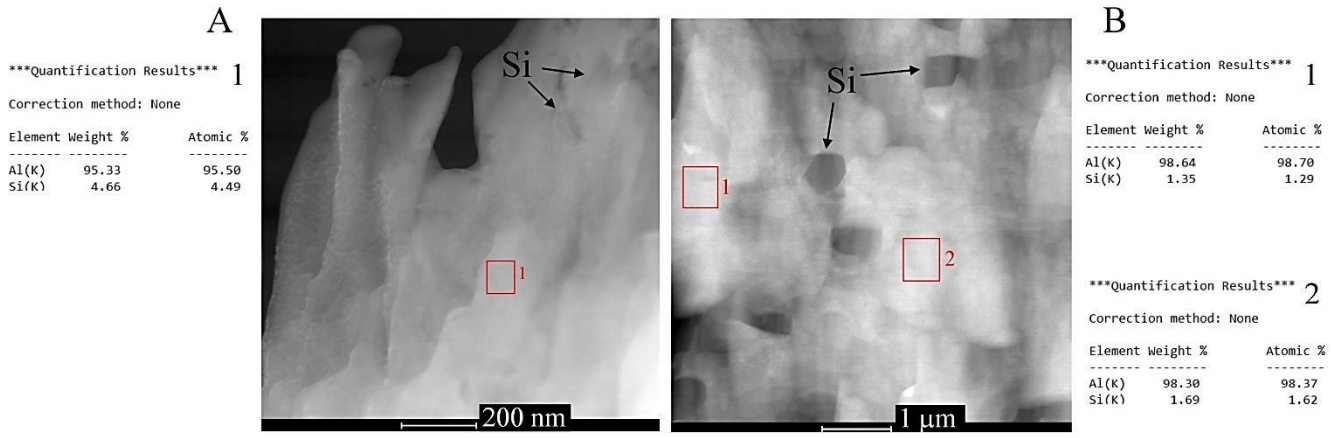

Fig. 5. STEM-HAADF images and EDS elemental analysis showing the Al and Si concentrations in α(Al) in the Al-12wt%Si specimens: (a) as-atomized condition (i.e., 0 min) and (b) after silicon spheroidization treatment at 813K for 6min.

C. Increments predicting strength

The microstructures of the as-atomized and as-heat treated samples for 1 min in Fig. 1 are associated with high strength based on the measured Vickers microhardnesses of 102 HV and 99 HV respectively in the Al-12wt% Si powders of size 355-425 μm, as can be seen in Fig. 6. In both cases, the fine eutectic mixture increases the mechanical strength. Indeed, the mentioned microhardness values are higher than the values reported by Haghdadi *et al.* [14], which examined thixocast A356 samples obtained at various periods at 540°C. In this case, the microhardness increased from 84 HV for 1 min to 87 HV for 2 min. In contrast, the present profile is much lower than those also reported by Haghdadi *et al.* [14] for severe plastic deformed (SPD) A356 samples, which reported 113 HV for 1 min to 102 HV for 2 min. Fig. 6 shows that after initial high hardness for 1 min, the alloy softens significantly due to the Si particles becoming coarser.

It is well known that the variations in hardness with microstructural parameter translating size can be given by $H=H_0+a\ (d)^{-b}$, where 'a' and 'b' are constants. The experimental exponent (-1/2) for the hardness-Si size relationship governing the rounded and fibrous silicon eutectic morphology found

in the present results was shown to be the same exponent as that adopted in other investigations on this regard [2,41].

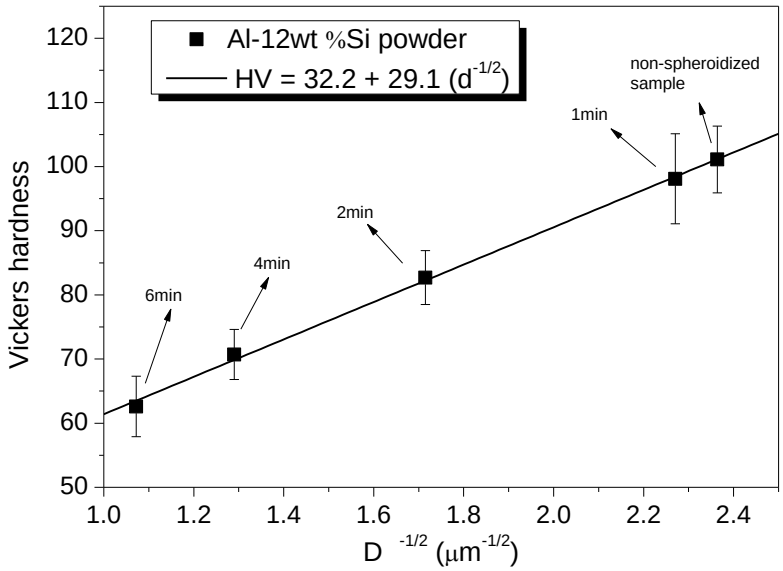

Fig. 6. Powder Vickers hardness (HV0.05 scale) as a function of the eutectic Si size found in the as-fabricated and annealed Al-12 wt% Si alloy samples.

The hardness tests were made over a sufficiently large area that encompassed all the phases present in the alloy. The sizes of the Vickers indent diagonals varied from 30μm to 42μm. As such, Vickers hardness may be utilized in increment method to estimate the yield strength

The strength increments approach is classified in three contributions, which are $\Delta\sigma_{ss}$, $\Delta\sigma_{Si}$ and $\Delta\sigma_{Al}$, as labelled inside Fig. 7. These values have been determined for each of the conditions examined in the investigated alloy, i.e., 0 min (as-fabricated sample), 1 min, 2 min, 4 min and 6 min. The contribution of each mechanism of strengthening can be properly evaluated for each microstructural condition. The strengthening of the eutectic Si appears as the most relevant in order to boost the strength, especially for the shorter treatment times. However, after longer heat treatments (i.e., 4 min and 6 min), only limited strength improvement may be related to $\Delta\sigma_{Si}$. The solid solution strengthening of Si, $\Delta\sigma_{ss}$, can also help to improve the strength. However, after the heat treatments for 4 min and 6 min, only limited amount of Si is left in the α-Al matrix as demonstrated in Fig. 4, and therefore, the strength input by Si solute in solution becomes limited.

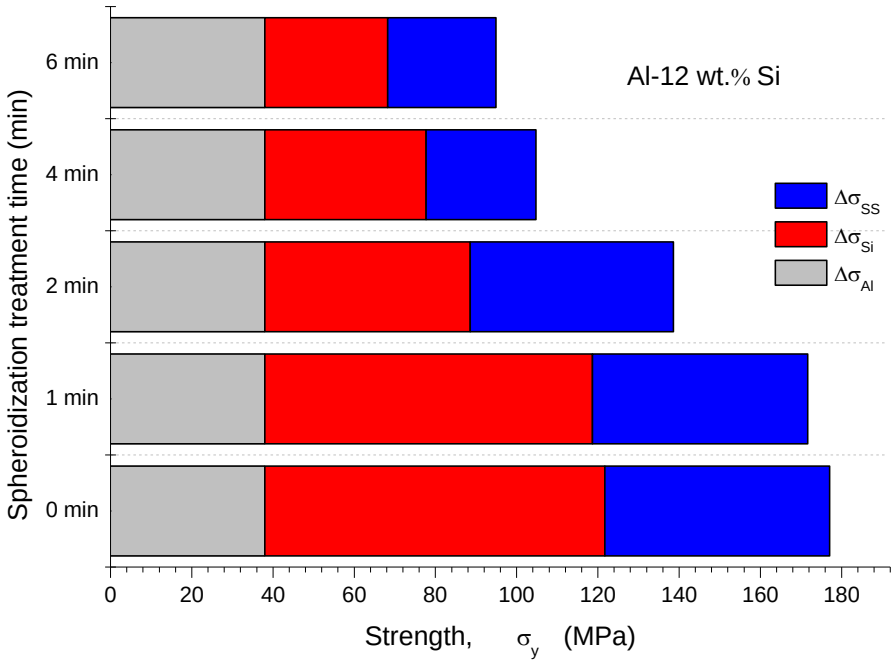

Fig. 7. Plot showing the contribution of each increment, that is, $\Delta\sigma_{ss}$, $\Delta\sigma_{Si}$ and $\Delta\sigma_{Al}$, composing the total yield strength predicted to the as-atomized and heat treated powder samples at 813K for various times.

The applicability of the increments methodology is further shown by comparing experimentally estimated and predicted strengths for the conditions investigated here, as can be seen in Fig. 8. The Vickers hardness, HV, measurements were utilized to estimate the yield strength by using the $\sigma_{y=0.2} = \frac{HV}{3} x(0.1)^{(m-2)}$, where 'm' is the Meyer's coefficient, which is 2.25 [42].

This model of increments predicts the strength of the IA heat treated Al-12wt %Si alloy powders with least deviations. Even though the comparisons show overall good agreement, the strength values can be considered slightly underpredicted for the samples treated for longer periods of time, that is, 4 min and 6min.

Contrasting this work with that of Lados et al [43] is of interest. Their samples including the Al-13Si-0.45 Mg with about 0.28Ti were cast. Heat treatments at 811K for 10 to 12 hours (T61 condition) were applied to the samples. The reported mechanical properties are shown not to degrade with time but gain an improvement from 260 MPa to about 310 MPa. This is considered to be due to the precipitation of Mg2Si precipitates. It follows then from our work that the combination of rapid

solidification and alloying particularly with Mg, should yield improved and non-degraded mechanical properties while utilizing fast heat treatment times. This is the subject of ongoing research.

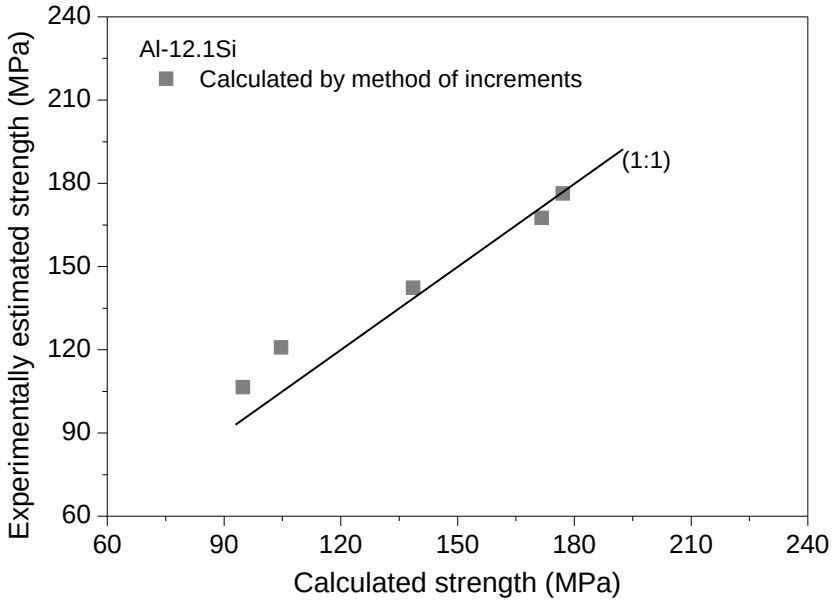

Fig. 8. Comparison between the experimentally estimated and the predicted yield strengths for the five conditions evaluated in this work in powder Al-12 wt% Si alloy: after atomization, after annealing treatments at 813K for 1 min, 2 min, 4 min and 6min.

4. Conclusions

The following outcomes can be outlined:

1. Fast treatments of the rapid solidified Al-12wt %Si powders at 813K for various short periods of time resulted in significant changes in the microstructure. Firstly, a gradual destruction of the dendritic pattern was observed after heat treatments until its complete absence for the 6 min sample. And secondly, the eutectic Si particles tended to transition from the coral to round shape and coarsened for exposure times from 1 min to 6 min. The heat treatment at 813K resulted in relative high hardness for 1 min, but for higher treatment time periods the material lost its strength significantly.

2. Eutectic Si network of the rapid solidified powders showed a fine dispersed coral fibrous architecture. This feature is considered to be very beneficial in order to improve the fragmentation

process during heat treatment of Al-Si alloys. The growth of Si in rods which branched into smaller cylinders was obtained through IA technique without adding doping elements.

3. The results from the present work highlight the applicability of the model of increments to predict strengths in Al-Si alloys. This is a useful approach needed to realize the full potential of rapid solidified Al-Si and Al-Si based alloys after being exposed to heat treatment process.

4. Very fine dispersion of eutectic Si fibers was generated by rapid solidification of the Al-12wt.%Si alloy. The mechanisms associated with the breakup of these fibers under heating were investigated vis-à-vis those established for other eutectics. The wavelength relative to the radius (r_0) of the Si fibers in the initial phase of heat treatment was 6.4 r_0 ±1.7, which favors the breakdown of rods and accelerate spheroidization. The volume diffusion of Si supersaturated in α-Al was another mechanism of spheroidization found in the present investigation.

Acknowledgements

The authors are grateful to FAPESP (São Paulo Research Foundation, Brazil: grants 2017/12741-6 and 2018/15059-4) for their financial support. This study was financed in part by the Coordenação de Aperfeiçoamento de Pessoal de Nível Superior - Brazil (CAPES). Support from the Natural Science and Engineering Research Council of Canada is also gratefully acknowledged.

References

[1] O. El Sebaie, A.M. Samuel, F.H. Samuel, H.W. Doty, The effects of mischmetal, cooling rate and heat treatment on the eutectic Si particle characteristics of A319.1, A356.2 and A413.1 Al-Si casting alloys, Mater. Sci. Eng. A 480 (2008) 342-355. Doi: 10.1016/j.msea.2007.07.039

[2] J.E. Spinelli, A.-A. Bogno, H. Henein, Two-Zone Microstructures in Al-18Si Alloy Powders, Metall. Mater. Trans. A 49 (2018) 550-562. Doi: 10.1007/s11661-017-4432-z

[3] J.W. Bray, ASM Handbook Volume 2: Properties and Selection: Nounferrous Alloys and Special-Purpose Materials, 10th ed., ASM Intl.: Cleveland, OH, USA, 1990, pp. 148. ISBN 0-87170-378-5.

[4] H. Elzanaty, Effect of composition on the microstructure, tensile and hardness properties of Al-xSi alloys, J. Mater. Sci. Surf. Eng. 2 (2015) 126-129. DOI-N: 10.jmsse/2348-8956/2-2.3

[5] M. Cohen, B.H. Kear, R. Mehrabian, Rapid solidification processing-An outlook. In Proceedings of the 2nd International Conference on Rapid Solidification Processing, Reston, VA, USA, 1980, pp. 1-25. http://www.dtic.mil/dtic/tr/fulltext/u2/a088473.pdf

[6] K.G. Prashanth, S. Scudino, H.J. Klauss, K.B. Surreddi, L. Löber, Z. Wang, A.K. Chaubey, U. Kuhn, J. Eckert, Microstructure and mechanical properties of Al-12Si produced by selective laser melting: Effect of heat treatment, Mater. Sci. Eng. A 590 (2014) 153-160. https://doi.org/10.1016/j.msea.2013.10.023

[7] G. Huiyuan, L. Yanxiang, C. Xiang, W. Xue, Effects of boron on eutectic solidification in hypoeutectic Al-Si alloys, Scripta Mater. 53 (2005) 69-73. https://doi.org/10.1016/j.scriptamat.2005.03.011

[8] F. Wang, Z. Liu, D. Qiu, J.A. Taylor, M.A. Easton, M. Zhang, Revisiting the role of peritectics in grain refinement of Al alloys, Acta Mater. 61 (2013) 360-370. https://doi.org/10.1016/j.actamat.2012.09.075

[9] L. Lu, K. Nogita, A.K. Dahle, Combining Sr and Na additions in hypoeutectic Al–Si foundry alloys, Mater. Sci. Eng. A 399 (2005) 244-253. https://doi.org/10.1016/j.msea.2005.03.091

[10] X.P. Li, X.J. Wang, M. Saunders, A. Suvorova, L.C. Zhang, Y.J. Liu, M.H. Fang, Z.H. Huang, T.B. Sercombe, A selective laser melting and solution heat treatment refined Al–12Si alloy with a controllable ultrafine eutectic microstructure and 25% tensile ductility, Acta Mater. 95 (2015) 74-82. https://doi.org/10.1016/j.actamat.2015.05.017

[11] A. Simar, S. Godet, T.R. Watkins, Highlights of the special issue on metal additive manufacturing, Mater. Charact. 143 (2018) 1-4. https://doi.org/10.1016/j.matchar.2018.06.013

[12] L. Zhou, A. Mehta, E. Schulz, B. McWilliams, K. Cho, Y. Sohn, Microstructure, precipitates and hardness of selectively laser melted AlSi10Mg alloy before and after heat treatment, Mater. Charact. 143 (2018) 5-17. https://doi.org/10.1016/j.matchar.2018.04.022

[13] M. Liu, H. Fu, C. Xu, W. Xiao, Q. Peng, H. Yamagata, C. Ma, Precipitation kinetics and hardening mechanism in Al-Si solid solutions processed by high pressure solution treatment, Mat. Sci. Eng. A 712 (2018) 757-764. https://doi.org/10.1016/j.msea.2017.12.033

[14] N. Haghdadi, A. Zarei-Hanzaki, M. Kawasaki, A.B. Phillion, P.D. Hodgson, Effect of Severe Plastic Deformation and Subsequent Silicon Spheroidizing Treatment on the Microstructure and Mechanical Properties of an Al–Si–Mg Alloy, Adv. Eng. Mater. 19 (2017) 1-8. https://doi-org.lama.univ-amu.fr/10.1002/adem.201700064

[15] E. Ogris, H. Lüchinger, P.J. Uggowitzer, Silicon Spheroidization Treatment of Thixoformed Al-Si-Mg Alloys, Mater. Sci. Forum 396-4 (2002) 149-154. https://doi.org/10.4028/www.scientific.net/MSF.396-402.149

[16] J.B. Wiskel, H. Henein, E. Maire, Solidification Study of Aluminum Alloys using Impulse Atomization: Part I: Heat Transfer Analysis of an Atomized Droplet, Can. Metall. Quart. 41 (2002) 97-110. https://doi.org/10.1179/cmq.2002.41.1.97

[17] A.-A. Bogno, P.D. Khatibi, H. Henein, Ch.-A. Gandin, Quantification of Primary Dendritic and Secondary Eutectic Nucleation Undercoolings in Rapidly Solidified Hypo-Eutectic Al-Cu Droplets, Metall. Mater. Trans. A 47A (2016) 4606-4615. DOI: 10.1007/s11661-016-3594-4

[18] M. Gündüz, E. Çadirli, Directional solidification of aluminium-copper alloys, Mater. Sci. Eng. A. 327 (2002) 167-185. Doi: 10.1016/S0921-5093(01)01649-5.

[19] E. Çadırlı, U. Büyük, S. Engin, H. Kaya, Effect of silicon content on microstructure, mechanical and electrical properties of the directionally solidified Al–based quaternary alloys, J. Alloys Compd. 694 (2017) 471–479. Doi:10.1016/j.jallcom.2016.10.010.

[20] H. Wen, Y. Lin, D.N. Seidman, J.M. Schoenung, I.J. van Rooyen, E.J. Lavernia, An Efficient and Cost-Effective Method for Preparing Transmission Electron Microscopy Samples from Powders, Microsc. Microanal. 21 (2015) 1184-1194. Doi: 10.1017/S1431927615014695

[21] Z. Li, Z. Zhang, X-G. CHEN, Effect of magnesium on dispersoid strengthening of Al-Mn-Mg-Si (3xxx) alloys, T. Nonferr. Metal Soc. 26 (2016) 2793-2799. Doi: 10.1016/S1003-6326(16)64407-2

[22] M.N. Shetty, Dislocations and Mechanical Behaviour of Materials, PHI Learning, Delhi, 2013, pp. 455. ISBN: 8120346386

[23] S. Roy, A. Wanner, Metal/ceramic composites from freeze-cast ceramic preforms: Domain structure and elastic properties, Compos. Sci. Technol. 68 (2008) 1136-1143. Doi: 10.1016/j.compscitech.2007.06.013

[24] T. Uesugi, Y. Takigawa, K. Higashi, Deformation Mechanism of Nanocrystalline Al-Fe Alloys by Analysis from Ab-Initio Calculations, Mater. Sci. Forum 503-504 (2006) 209-214. DOI: 10.4028/www.scientific.net/MSF.503-504.209

[25] T. Suzuki, S. Takeuchi, H. Yoshinaga, Dislocation dynamics and plasticity, first edition, in: U. Gonser (Ed.), Springer Series in Materials Science, Springer-Verlag, New York, 1991, pp. 32-44. ISBN 978-3-642-75774-7

[26] MatWeb, Material Property Data. http:// http://www.matweb.com/search/PropertySearch.aspx, (accessed 05 September 2018).

[27] V.C. Srivastava, R.K. Mandal, S.N. Ojha, Microstructure and mechanical properties of Al-Si alloys produced by spray forming process, Mater. Sci. Eng. A 304 (2001) 555-558. DOI: 10.1016/S0921-5093(00)01514-8

[28] R.V. Reyes, R. Kakitani, T.A. Costa, J.E. Spinelli, N. Cheung, A. Garcia, Cooling thermal parameters, microstructural spacing and mechanical properties in a directionally solidified hypereutectic Al-Si alloy, Phil. Mag. Lett. 96 (2016) 228-237. DOI: 10.1080/09500839.2016.1192297

[29] M. Glazoff, V. Zolotorevsky, N. Belov, Casting Aluminum Alloys, Influence of Heat Treatment: Microstructure of Casting Al Alloys, first edition, Elsevier Science, 2007, pp. 213-222. ISBN: 9780080453705

[30] S. Hegde, K.N. Prabhu, Modification of eutectic silicon in Al-Si alloys, J. Mater. Sci. 43 (2008) 3009-3027. Doi: 10.1007/s10853-008-2505-5

[31] ASM Handbook Volume 15: Casting, 9th ed., Solidification of Eutectic Alloys: Aluminum-Silicon Alloys, ASM Intl.: Cleveland, OH, USA, 1992. ISBN: 978-0-87170-711-6

[32] E. Ho, G.C. Weatherly, Interface Diffusion In The Al-CuAl2 Eutectic, Acta Metall. 23 (1975) 1451-1460. Doi: 10.1016/0001-6160(75)90154-6

[33] E. Ho, G.C. Weatherly, The thermal stability of deformed Al-$CuAl_2$ eutectic, Met. Sci. 11 (1977) 109-116. Doi: 10.1179/msc.1977.11.4.109

[34] K.T. Conlon, E. Maire, D.S. Wilkinson, H. Henein, Processing and Microstructural Characterization of Al-Cu Alloys Produced from Rapidly Solidified Powders, Metall. Mater. Trans. A 31A (2000) 249-260. DOI: 10.1007/s11661-000-0069-3

[35] G.C. Weatherly, Treatise on Materials Science and Technology, The Stability of Eutectic Microstructures at Elevated Temperatures, first edition, Academic Press, Volume 8, 1975, pp. 121-175. ISBN: 9781483218175

[36] G. Sharma, R.V. Ramanujan, G.P. Tiwari, Instability Mechanisms In Lamellar Microstructures, Acta Mater. 48 (2000) 875-889. DOI: 10.1016/S1359-6454(99)00378-X

[37] S. Taktak, H. Akbulut, Diffusion kinetics of explosively treated and plasma nitrided Ti-6Al-4V alloy, Vacuum 75 (2004) 247-259. DOI: 10.1016/j.vacuum.2004.03.004

[38] S.P. Ding, W.T. Petuskey, Solutions to Fick's second law of diffusion with a sinusoidal excitation, Solid State Ionics 109 (1998) 101-110. DOI: 10.1016/S0167-2738(98)00103-9

[39] T. Ujihara, K. Fujiwara, G. Sazaki, N. Usami, K. Nakajima, New method for measurement of interdiffusion coefficient in high temperature solutions based on Fick's first law, J. Cryst. Growth 241 (2002) 387-394. DOI: 10.1016/S0022-0248(02)01316-7

[40] S.N. Samaras, G.N. Haidemenopoulos, Modelling of microsegregation and homogenization of 6061 extrudable Al-alloy, J. Mater. Process Technol. 194 (2007) 63-73. DOI: 10.1016/j.jmatprotec.2007.03.126

[41] S. Khan, A. Ourdjini, Q.S. Named, M.A. Alam Najafabadi, R. Elliott, Hardness and mechanical property relationships in directionally solidified aluminium-silicon eutectic alloys with different silicon morphologies, J. Mater. Sci. 28 (1993) 5957-5962. DOI: 10.1007/BF00365208

[42] J.R. Cahoon, W.H. Broughton, A.R. Kutzak, The Determination of Yield Strength From Hardness Measurements, Metall. Mater. Trans. B 2 (1971) 1979-1983. Doi: 10.1007/BF02913433

[43] D.A. Lados, D. Apelian and L. Wang, Aging Effects on Heat Treatment Response and Mechanical Properties of Al-(1-13 pct)Si-Mg Cast Alloys, Metall. Mater. Trans B 42 (2011) 181-188. DOI: 10.1007/s11663-010-9438-5

List of Figure Captions

Fig. 1. Representative (a) OM, (b) light-etched SEM and (c) deep-etched SEM micrographs of the as-atomized and heat treated Al-12 wt% Si alloy specimens for different heat treatment times.

Fig. 2. Variation in range of the Si spacing (λ) and Si size (D) as a function of the annealing treatment at 813K for various times, t, for the Al-12 wt%Si of size 355-425µm generated by impulse atomization under helium atmosphere.

Fig. 3. Plot showing comparison between the Si size with time in the present investigation (i.e., rapid solidified powders) and those found in the literature for the A356 Al alloy generated under different manufacturing routes. Solid and dash-dot lines are from ref. [14].

Fig. 4. (a) SEM images through SE mode indicate the evaluated microprobe points emphasizing the composition of the α-Al area within the microstructures. (b) Experimental variation of silicon content in solid solution of the as-tested Al-12 wt% Si alloys samples corresponding to treatment at 813K for various times (i.e., A - 0min; B - 1min; C - 4min and D - 6min). (c) Variation of RMS diffusion distance of Si in α(Al) with treatment time.

Fig. 5. STEM-HAADF images and EDS elemental analysis showing the Al and Si concentrations in α(Al) in the Al-12wt%Si specimens: (a) as-atomized condition (i.e., 0 min) and (b) after silicon spheroidization treatment at 813K for 6min.

Fig. 6. Powder Vickers hardness (HV0.05 scale) as a function of the eutectic Si size found in the as-fabricated and annealed Al-12 wt% Si alloy samples.

Fig. 7. Plot showing the contribution of each increment, that is, $\Delta\sigma_{ss}$, $\Delta\sigma_{Si}$ and $\Delta\sigma_{Al}$, composing the total yield strength predicted to the as-atomized and heat treated powder samples at 813K for various times.

Fig. 8. Comparison between the experimentally estimated and the predicted yield strengths for the five conditions evaluated in this work in powder Al-12 wt% Si alloy: after atomization, after annealing treatments at 813K for 1 min, 2 min, 4 min and 6min.